Journal of Applied Fluid Mechanics, Vol. 17, No. 1, pp. 192-204, 2024.
Available online at www.jafmonline.net, ISSN 1735-3572, EISSN 1735-3645.
https://doi.org/10.47176/jafm.17.1.1998

Dynamic Modeling and Combination Analysis of Plunger Valve Considering Both Flow and Actuator

Y. Ren[1], C. Bai[1†] and H. Zhang[2]

[1] *State Key Laboratory for Strength and Vibration of Mechanical Structures / Shaanxi Key Laboratory of Environment and Control for Flight Vehicle, Xi'an Jiaotong University, Xi'an 710049, China*
[2] *School of Science, Chang'an University, Xi'an 710064, China*

†*Corresponding Author Email: baichq@mail.xjtu.edu.cn*

ABSTRACT

The plunger valve has an important role in a large compressor system as its operating characteristics directly affect the aerodynamic boundary condition of the compressor equipment. In this study, dynamic modeling and analysis method of the plunger valve are proposed for an accurate control of the system. By considering the interaction between the dynamic flow in the valve and actuator action, a lumped parameter model for the fluid–structure interaction force and multibody dynamic model of the actuator are developed based on intrinsic correlation parameters. A combination analysis to simultaneously predict valve flow and actuator dynamic characteristics is proposed. The predicted results are in a good agreement with experimental data, which validates the proposed model and analysis method. The analysis results show that the coupling effect between the valve flow and actuator is significant and has an important role in valve control, particularly when the valve opening is smaller. Compared to the experimental data and computational fluid dynamics results, the presented methods are accurate for valve control and effective for prediction of flow rate.

Article History

Received May 14, 2023
Revised August 10, 2023
Accepted August 31, 2023
Available online November 1, 2023

Keywords:

Plunger valve
Actuator
Dynamic model
Combination analysis
Flow characteristics

1. INTRODUCTION

Plunger valves, as important equipment for regulation of pressure, flow rate, and liquid level, are commonly used to maintain constant flow rate and pressure in a compressor system. They have been widely applied in aerospace, hydraulic engineering, chemical, and other engineering fields owing to numerous advantages such as the large flow capacity and anti-cavitation. The flow area of the plunger valve can be changed to adjust the flow in the compressor system during the actuator operation. The flow rate and pressure in the valve fluctuate with the changing opening, affecting the compressor operation stability. The accurate flow rate control of the plunger valve is closely related to the motion of the actuator and dynamic flow in the valve. Therefore, a dynamic analysis considering both flow and actuator is important in determination of the flow rate of the plunger valve. It is also a key problem that must be solved in the accurate control of the compressor system.

Previous studies have provided insights into the flow characteristics of the plunger-type valve. The research approaches for the flow characteristics are mainly limited to computational fluid dynamics simulations and experimental tests. Wang et al. (2016) developed a plunger valve model and conducted a finite-element static analysis, safety factor testing, and fluid–structure coupling analysis. Prasad et al. (2011) carried out a numerical flow simulation of plunger valves with and without orifice plates at seven different valve openings. They investigated the valve characteristics, such as head loss, flow rate, and cavitation coefficient, under different operating conditions. A method for evaluation of the presence of cavitation during the operation of a pressure-reducing valve in a water distribution system has been proposed by Ulanicki et al. (2015). To decrease the cavitation in plunger valves, Wang et al. (2018) analyzed the difference between flow simulation calculations of a monolayer plunger valve and double plunger valve at a low backpressure and high pressure difference, and showed that the double plunger valve is more effective in decreasing the cavitation. Based on an experimental research, Zheng et al. (2019) proposed flow control approaches to study the erosion characteristics of an axial flow regulating valve and verified their validity by numerical simulations. Saha et al. (2014) used a computational fluid dynamics technique to study dynamic modeling of flow processes inside a pressure-regulating

NOMENCLATURE

A_p	effective area of hydraulic cylinder piston	Q_m	mass flow rate
B_p	viscous damping coefficient	Q_v	volume flow rate of the plunger valve
C	contraction coefficient of the orifice	S_1	areas of the windows
C_{ep}	external leakage coefficients of the hydraulic cylinder	S_2	areas of the vena contracta
C_{ip}	internal leakage coefficients of the hydraulic cylinder	S_{in}	area of the pipe inlet
C_{tp}	total leakage coefficient	S_p	low pressure area of the plunger
D	inside diameter of the outlet pipe	u	fluid velocity of the vena contracta of the orifice flow
F	external load	V_t	total compression volume
F_L	force from transmission mechanism	x_p	displacements of the hydraulic piston
F_p	FSI force	x_v	displacements of the spool
K	elastic coefficient of the load	x_w	plunger position
K_{ce}	total flow rate-pressure coefficient	β_ε	liquid bulk modulus
K_q	flow gain of spool	γ	specific heats ratio of the air
K_c	flow gain of spool	θ	the divergence angle of the diffuser
L_1	length of valve channel behind the windows	κ	wall roughness
L_2	length of the pipe connected to the outlet	λ	frictional drag coefficient
$\overline{Ma}$	nominal Mach number	μ_1	total resistance coefficient along the flow path
p_0	pressure of the orifice upstream	μ_2	total local resistance coefficient
p_2	pressure of the vena contracta	ξ_d	local resistance coefficient at the diffuser
p_{in}	pressure of the inlet	ξ_e	local resistance coefficient at the elbow
p_{left}	pressure of the left cavity	ξ_{sv}	damping ratio of the electro-hydraulic servovalve
P_L	pressure drop of load	ρ_0	density of the orifice upstream
p_{right}	pressure of the right cavity	ρ_2	fluid density of the vena contracta flow
p_r	pressure ratio	ω	natural frequency of the electro-hydraulic servovalve
p_R	oil spill pressure	ΔI	control current of the electro-hydraulic servovalve
p_{out}	pressure of the pipe outlet	Δp_λ	pressure drop caused by friction drag
p_s	oil feed pressure	Δp_ξ	local pressure drop
q_1	oil feed flow rate	Δp	pressure drop
q_2	oil spill flow rate	Q_m	mass flow rate
Q_0	flow rate of the no-load state	Q_v	volume flow rate of the plunger valve
Q_L	flow rate of the spool		

and shut-off valve and predicted the spool movement and final spool position when the spool position departed from equilibrium. Yu and Yu (2015) investigated the flow and sound fields of an axial flow check valve through simulation and experimental methods, and demonstrated that the streamlined design applied to the main channel structure of the valve body can reduce the maximum noise and spool resistance coefficient. These studies indicated that numerical simulations and experimental tests are effective approaches to obtain the dynamic properties of the plunger valve, but coupling effects between the plunger valve and actuator were not considered. Thus, the research results cannot be directly used for valve control.

Hydraulic actuator, which has a key role in valve control, is utilized in industrial applications requiring overload capacity, robustness, and high dynamic performance. By replacing the torque motor, Karunanidhi and Singaperumal (2010) developed and integrated a magnetostrictive actuator into an existing flapper-nozzle servo valve. They incorporated the magnetostrictive actuator dynamics into a valve dynamics simulation. Kim et al. (2012) presented an output feedback nonlinear control for position tracking of electro-hydraulic systems and validated the proposed approach through simulations and experiments. A discontinuous projection-based ARC controller has been constructed by Yao et al. (2001) for a high-performance robust motion control of a typical one-degree-of-freedom electro-hydraulic servo system driven by a double-rod hydraulic cylinder. Gupta et al. (2019) used MATLAB Simulink to explore the design analysis of a nonlinear electro-hydraulic servo system and displacement control at different combinations of frequencies of a symmetric double-acting hydraulic actuator. Aboelela et al. (2018) constructed a nonlinear simulation model of a hydraulic servo system based on physical laws and experimental piston position identification. Ferrari et al. (2018) developed a numerical model of a servo actuator and four-port proportional direction control valve, which was validated based on the experimental time history of the actuator speed and flow rate controlled by the proportional valve.

Although extensive experiments and simulations have been carried out on electro-hydraulic servo actuators, only a few studies have coupled the flow in the valve with the

actuator. Naseradinmousavi and Nataraj (2011) used multiphysics models to conduct modeling and analysis of the opening and closing processes of butterfly valves driven by solenoid actuators. A multiphysics coupled model was developed by Xiong et al. (2019) to evaluate the performance of an energy coupler actuator used for a high-speed valve. There are scarce reports related to the valve–actuator coupling relationship, although the coupling relationship is important for an accurate valve control.

The aim of this study was dynamic modeling and combination analysis of the plunger valve and its actuator. A lumped parameter model is presented to explore the fluid–structure interaction (FSI) force and flow rate of the plunger valve. A multibody dynamics model of the actuator is then established based on the fundamental equations of the hydraulic cylinder and three-dimensional (3D) modeling of the transmission mechanism. A combined analysis procedure is proposed on this basis. The presented method is verified by comparing it to experimental results.

2. Dynamic Modeling for Flow and Actuator of Plunger Valve

The plunger valve is composed of a valve body, valve shaft, cranks, plunger, and guide cap, as shown in Fig. 1. At the end of the guide cap, 12 cup-shaped windows are uniformly distributed. The plunger is driven by the actuator via the transmission mechanism and resists the pressure from the flow field. The window areas of the valve, which are determined by the corresponding positions of the plunger, could significantly affect flow parameters, such as the flow resistance, pressure drop, and flow rate.

As shown in Fig. 1(a), the plunger location, determined by the actuator, is directly related to the flow regime and flow rate of the valve. The flow field exerts the FSI force applied to the plunger and transmitted to the actuator. Therefore, the drive performance of the actuator is affected by the transmitted force, leading to an impact on the location control of the plunger. This indicates that the plunger valve and actuator affect and correlate with each other. A combination analysis considering both flow and actuator is necessary to accurately predict the flow rate. Dynamic modeling with coupling effects is required for the combination analysis. The lumped parameter model of FSI force and multibody dynamic model of the actuator are presented in Sections 2.1 and 2.2, respectively.

2.1 Lumped Parameter Modeling for FSI Force

When the plunger moves to a certain location, the axial cross section of the flow channel is shown in Fig. 1(a), where D is the inside diameter of the outlet pipe, L_1 is the valve channel length behind the windows, and L_2 is the length of the pipe connected to the outlet.

As the area of the valve window is considerably smaller than the valve inlet, the valve window can be equivalent to a thin orifice plate. Sudden contraction and

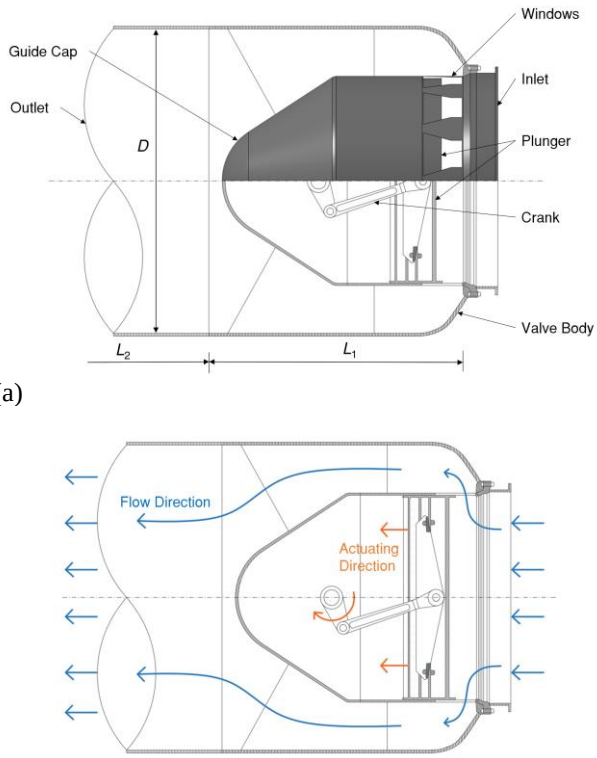

Fig. 1 Schematic diagram of the plunger valve (a) Structural model (b) Flow and actuating direction

expansion occur when the fluid flows through the valve windows. As shown in Fig. 1(b), the internal flow field of the plunger valve curves along the valve channel. The flow channel behind the valve windows could be divided into three parts, Channels A, B, and C, as shown in Fig. 2. According to their flow characteristics, Channels A, B, and C could be simplified as an elbow, diffuser, and constant-cross-section friction pipe, respectively. A schematic of flow channel decomposition is presented in Fig. 2.

The pressure drop behind the valve windows includes that caused by friction drag and local pressure drop. When the flow is steady, the pressure drop, denoted as Δp, can be expressed as:

$$\Delta p = \Delta p_{\lambda} + \Delta p_{\xi} \tag{1}$$

where Δp_{λ} is the pressure drop caused by friction drag and Δp_{ξ} is the local pressure drop.

The frictional drag of Channels A, B, and C can be determined by the wall roughness, κ, and Reynolds number, *Re*, which primarily includes the pipe wall friction and friction between flow layers. The airflow in the plunger valve is deemed turbulent when the valve airflow velocity is so high that the airflow Reynolds number exceeds 4×10^3. The relationship employed in this study is based on the well-known Colebrook–White expression (Valiantzas, 2008):

$$\frac{1}{\sqrt{\lambda}} = 2\log\left[\frac{Re\sqrt{\lambda}}{2.51} + \frac{3.7D}{\kappa}\right] \tag{2}$$

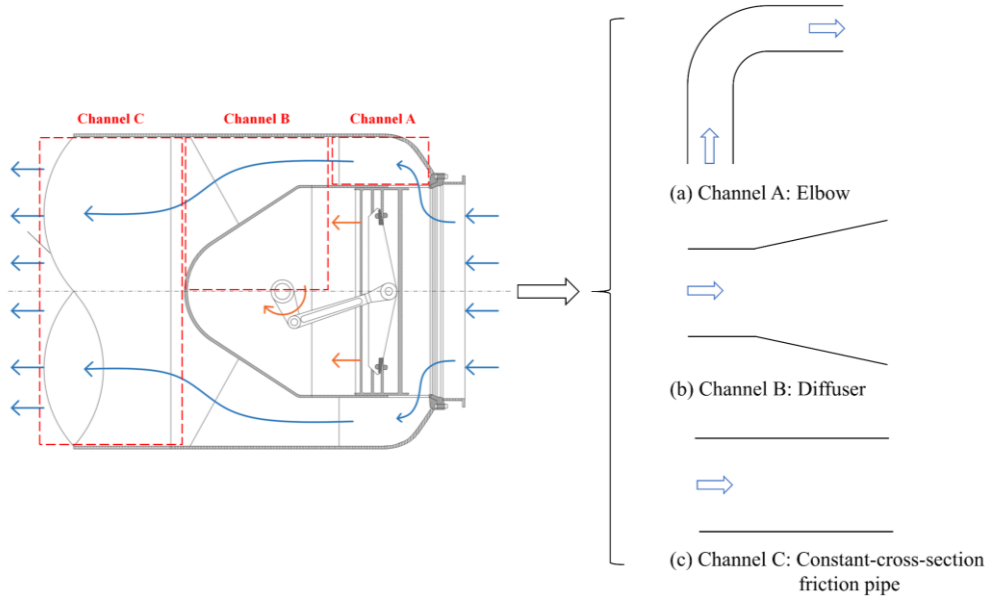

Fig. 2 Schematic diagram of flow channel decomposition

where λ is the frictional drag coefficient, D is the inside diameter of the outlet pipe, and κ is the wall roughness.

The Darcy–Weisbach formula (Valiantzas, 2008) can be employed to calculate the total coefficient along the flow path, $\mu_1 = \lambda[(L_1 + L_2)/D]$. The pressure drop caused by friction drag can be expressed as

$$\Delta p_\lambda = \frac{\mu_1 \rho_2 u^2}{2} = \frac{\lambda(L_1 + L_2)\rho_2 u^2}{2D} \tag{3}$$

where ρ_2 is the fluid density of the vena contracta flow and u is the fluid velocity of the vena contracta of the orifice flow, as shown in Fig. 3.

The airflow bends in Channel A due to the blockage of the wall, forming an elbow. According to the study by Morimune et al. (1980), the local resistance coefficient at the elbow can be calculated by $\xi_e = 1.05 + 7.2\overline{Ma}^{3.17}$, where $\overline{Ma}$ is the nominal Mach number. The cross-sectional area of Channel B expands gradually along the flow direction, resulting in vortices and flow resistance there. Therefore, Channel B is equivalently simplified as a diffuser. Through experiments and computational fluid dynamics methods, Gan and Riffat (1996) obtained the correlation formula of the local resistance coefficient at the diffuser: $\xi_d = a_0 + a_1\theta + a_2\theta^2 + a_3\theta^3 + a_4\theta^4 + a_5\theta^5$, where θ is the divergence angle of the diffuser and a_i are constant parameters. The total local resistance coefficient can be obtained by analyzing the equivalent resistance coefficients of Channels A and B: $\mu_2 = \xi_e + \xi_d$. The local pressure drop can be expressed as

$$\Delta p_\xi = \frac{\mu_2 \rho_2 u^2}{2} = \frac{(\xi_e + \xi_d)\rho_2 u^2}{2} \tag{4}$$

Both pressure drop behind the windows, Δp, and pressure of the vena contracta, p_2, can be characterized by u:

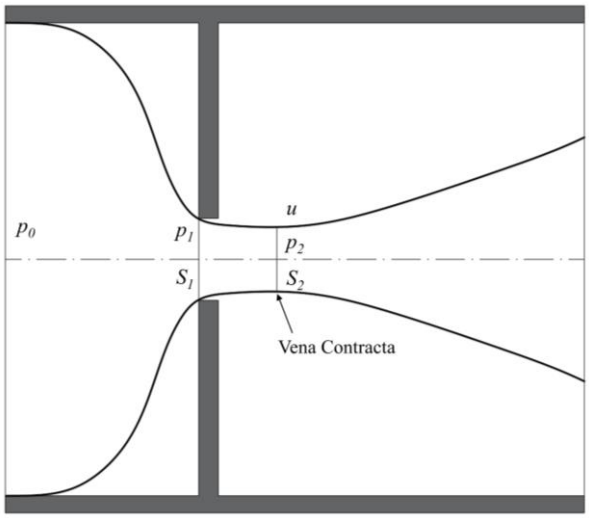

Fig. 3 Schematic of airflow through an orifice

$$\Delta p = \frac{(\mu_1 + \mu_2)\rho_2 u^2}{2} \tag{5}$$

$$p_2 = p_{out} + \Delta p \tag{6}$$

where p_{out} is the pressure of the pipe outlet.

The fluid medium in the valve is isentropic and can be considered as a compressible ideal gas. According to the Poisson's formula and ideal gas state equation, the relationship between ρ_2 and p_2 can be expressed as

$$p_0 \rho_0^{-\gamma} = p_2 \rho_2^{-\gamma} \tag{7}$$

where p_0 and ρ_0 are the pressure and air density of the orifice upstream, respectively.

As mentioned, the valve window can be approximately deemed to be an orifice. After a distance, the airflow via the window reaches the vena contracta. The contraction coefficient of the orifice is defined as

$C = S_2 / S_1$, varying with the valve operating condition, where S_1 and S_2 are the areas of the windows and vena contracta of the airflow, respectively. The area ratio of the windows and inlet can be expressed as $\delta = S_1 / S_{in}$, where S_{in} is the area of the pipe inlet. The contraction coefficients under different Reynolds numbers and pressure ratios, P_r, are compared in Fig. 14 of Appendix A.

The volume flow rate of the plunger valve, Q_v, can be expressed as:

$$Q_v = S_2 u = C S_1 u \tag{8}$$

The fluid velocity at the vena contracta can be obtained by the Saint-Venant and Wantzel formula (Jobson, 1955):

$$u = \sqrt{\frac{P_{in}}{\rho_0}\frac{2\gamma}{\gamma-1}\left(\frac{P_2}{P_{in}}\right)^{2/\gamma}\left[1-\left(\frac{P_2}{P_{in}}\right)^{\gamma-1/\gamma}\right]} \tag{9}$$

where P_{in} is the pressure of the inlet and γ is the specific heat ratio of the air. According to Eqs. (6), (7), and (9), the velocity of the vena contracta can be derived. Therefore, the mass flow rate of the plunger valve can be expressed as

$$Q_m = \rho_2 Q_v = \rho_2 C S_1 u \tag{10}$$

The movement of the plunger leads to a change in the flow state, while the airflow exerts an FSI force on the plunger. There is an equalizing pressure chamber inside the guide cap due to the blocking effect of the windows. Therefore, the plunger pressure on the guide cap side is equivalent to the inlet pressure, P_{in}. In contrast, a low-pressure area emerges on the window side of the plunger because of the high-speed airflow in the window region. Therefore, there is a pressure difference across the plunger. Because the airflow shrinks after the window, the flow shape is considered as a reducer, where the pressure loss coefficient is insignificant, and thus can be ignored (Finnemore & Franzini, 2002). Thus, p_1 is approximately p_2. The pressure difference causes the FSI force F_p of the plunger, which may be expressed as

$$F_p = S_p(p_{in} - p_1) \tag{11}$$

where S_p is the low-pressure area of the plunger. The lumped parameter modeling process for FSI force is shown in Fig. 4.

2.2 Multibody Dynamics Modeling for Plunger Valve Actuator

The plunger valve actuator usually consists of a hydraulic pump station, electro-hydraulic servo valve, hydraulic cylinder, displacement sensor, transmission mechanism, etc. In the transmission mechanism, the linear movement of the rack, which is linked by the hydraulic piston, rotates the gear. The valve shaft, which is fixedly attached to the gear, then powers the crank to alter the valve opening. Owing to the characteristics of the hydraulic servo system, some problems, such as response lag and oscillation, exist in the process of flow adjustment. Thus, multibody dynamics modeling is needed to investigate the input–output response of the actuator.

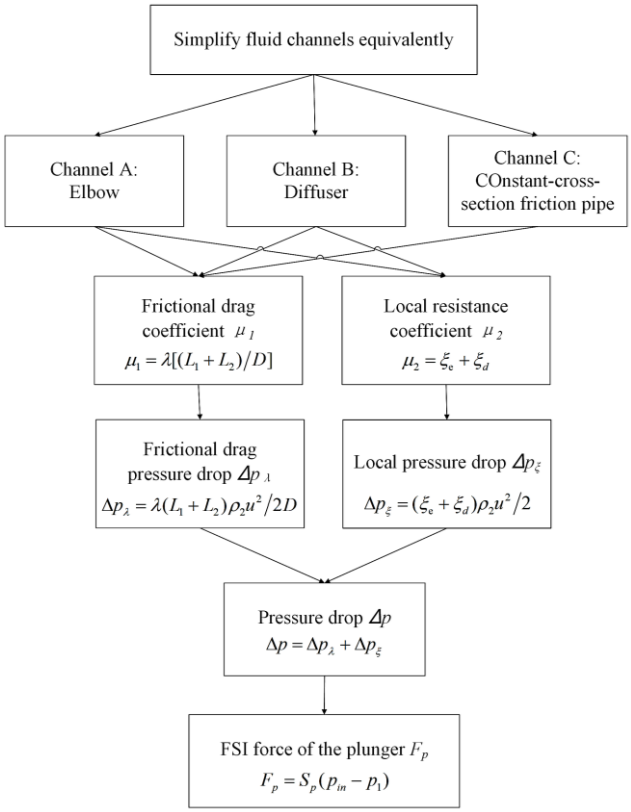

Fig. 4 Lumped parameter modeling process for FSI force

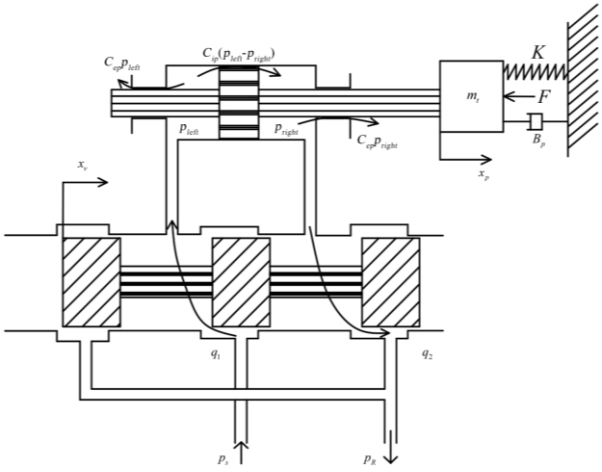

Fig. 5 Schematic diagram of valve-controlled hydraulic cylinder

The hydraulic servo system can be simplified to a standard valve-controlled hydraulic cylinder (Yao et al., 2000). The hydraulic cylinder is axisymmetric and controlled by a four-way valve. Its functional diagram is shown in Fig. 5 (Shao et al., 2005), where x_v and x_p are the displacements of the spool and hydraulic piston, respectively, C_{ep} and C_{ip} are the external and internal leakage coefficients of the hydraulic cylinder, p_{left}, p_{right}, p_s, and p_R are the pressure of the left cavity, pressure of the right cavity, oil feed pressure, and oil spill pressure,

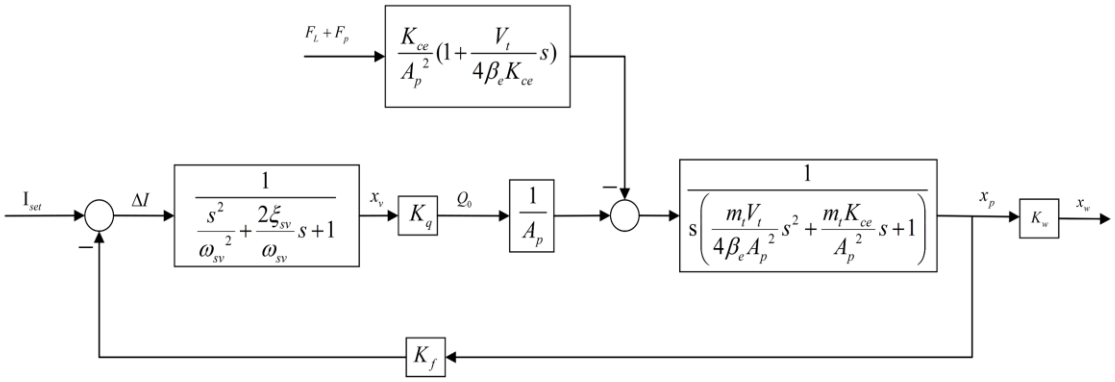

Fig. 6 Closed-loop control procedure of plunger displacement

respectively, q_1 and q_2 are the oil feed flow rate and oil spill flow rate, respectively, m_t is the equivalent total mass of the piston and load, B_p is the viscous damping coefficient of the piston rod and load, K is the elastic coefficient of the load, and $F = F_L + F_p$ is the external load, where F_L is the force from the transmission mechanism to the hydraulic piston, which can be expressed as a function of the hydraulic piston displacement, $F_L = f(x_p)$.

To describe the dynamic characteristics of the hydraulic cylinder, the Laplace transforms of the flow equation of the hydraulic control valve, continuity equation of the hydraulic cylinder, and equilibrium equation of the hydraulic cylinder and load force are expressed as

$$Q_L = K_q x_v - K_c P_L \tag{12}$$

$$Q_L = A_p x_p s + C_{tp} P_L + \frac{V_t}{4\beta_\varepsilon} P_L s \tag{13}$$

$$A_p P_L = m_t x_p s^2 + B_p x_p s + K x_p + F \tag{14}$$

where Q_L is the flow rate of the spool, K_q and K_c are the flow gain of the spool and flow-pressure coefficient of the spool, respectively, P_L is the pressure drop of the load, β_ε is the liquid bulk modulus, A_p is the effective area of the hydraulic cylinder piston, C_{tp} is the total leakage coefficient, $C_{tp} = C_{ip} + C_{ep}$, and V_t is the total compression volume. According to Eqs. (12)–(14), the output displacement of the hydraulic cylinder piston, x_p, can be expressed as

$$x_p = \frac{\frac{K_q}{A_p}x_v - \frac{K_{ce}}{A_p^2}(1+\frac{V_t}{4\beta_e K_{ce}}s)(F_L+F_p)}{\frac{m_t V_t}{4\beta_e A_p^2}s^3 + (\frac{m_t K_{ce}}{A_p^2}+\frac{B_p V_t}{4\beta_e A_p^2})s^2 + (1+\frac{B_p K_{ce}}{A_p^2}+\frac{K V_t}{4\beta_e K_{ce}})s + \frac{K K_{ce}}{A_p^2}} \tag{15}$$

where K_{ce} is the total flow rate-pressure coefficient, $K_{ce} = K_e + K_{tp}$. The viscous damping coefficient of the load is small, the load can be considered as a rigid body, and thus B_p and K can be ignored.

The transfer function of the servo valve can be approximated to a second-order oscillation,

$$\frac{Q_0}{\Delta I} = \frac{K_q}{\frac{s^2}{\omega_{sv}^2}+\frac{2\xi_{sv}}{\omega_{sv}}s+1} \tag{16}$$

where Q_0 is the flow rate of the no-load state, ΔI is the control current of the electro-hydraulic servo valve, ω is the natural frequency of the electro-hydraulic servo valve, and ξ_{sv} is the damping ratio of the electro-hydraulic servo valve. The displacement relationship between the piston and plunger can be approximated to be linear. The displacement sensor linearly converts the displacement data of the hydraulic piston into the electrical signal, so that the conversion process can be regarded as a proportional component, as presented by K_f. The closed-loop control procedure is illustrated in Fig. 6, where x_p is the displacement of the hydraulic cylinder piston. Therefore, the window area ratio, δ, is obtained according to the corresponding relationship between the window shape and plunger position determined by x_w.

3. COMBINATION ANALYSIS FOR PLUNGER VALVE

Based on the dynamic models established above, a combination analysis for the flow and actuator of the plunger valve can be proposed. The lumped parameter model and multibody dynamics model of the actuator are combined through the FSI force and coupling effect. Thus, the combination analysis method can be presented for the coupling solution of fluid flow and actuator action, realizing the process from the actuator signal input to the flow rate output. The steps of the combination analysis are as follows.

1) Initialization. The electrical signal is first sent into the controller, and the initial window area ratio is obtained as a result. The mass flow rate is then given an initial value based on the empirical relationship. The nominal Mach number of the window can be calculated by the ratio of the initial mass flow rate to the window area, which will be utilized in the following phase for lumped parameter modeling.

2) Lumped parameter modeling for FSI force. Behind the valve windows, the channels are reasonably

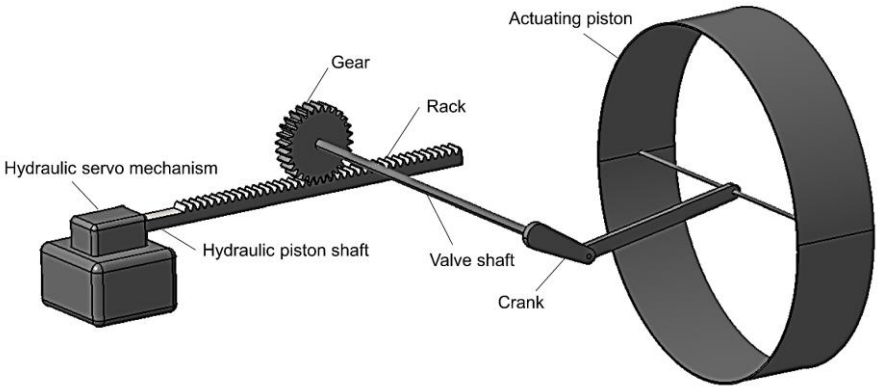

Fig. 7 Schematic diagram of plunger valve hydraulic servo-transmission mechanism

3) simplified into some elements. The pressure drop behind the windows includes the local pressure drop and frictional drag pressure drop. The local drag coefficients of elbows and diffusers are calculated using the empirical formula. The drag coefficient along the path is calculated using the Colebrook–White formula. The difference between the outlet pressure and pressure drop represents the pressure at the window side of the plunger. The FSI force of the plunger is computed by multiplying the pressure difference by the plunger area of low pressure. Simultaneously, the Saint Venant–Wantzel formula is employed to calculate the vena contracta velocity of the stream, and then the flow rate of the valve can be calculated.

4) Multibody dynamics modeling of the actuator. 3D modeling, assembly, and dynamic analysis of the transmission mechanism are carried out. The relationship between the displacement of the hydraulic cylinder piston and external force is then derived by a simulation. The simplified theoretical equation of the hydraulic servo system is used to develop the transfer function equation of the piston cylinder and servo valve. Using Matlab/Simulink, the external force of the actuator is substituted into the mathematical model. The window area ratio may be calculated by linearly converting the output displacement of the hydraulic piston cylinder to the displacement of the plunger.

5) Error judgment of the window area ratio. When the relative error between the window area ratio and initial value exceeds the specified maximum error, the window area ratio is returned as the initial value for an iterative calculation. Otherwise, the calculation will proceed to the next steps.

6) Calculation of the mass flow rate. By inputting the contraction coefficient of the relevant working state into the formula, the mass flow rate of the valve is computed.

7) Error judgment of the mass flow rate. It is returned as the initial mass flow rate for an iterative computation when the relative error between the flow rate acquired in the previous step and initial flow rate exceeds the specified maximum error. Otherwise, the ultimate mass flow rate is output.

Figure 13 in Appendix A presents a flowchart for the combined analysis approach mentioned above.

4. VERIFICATION AND DISCUSSION OF THE COMBINATION ANALYSIS

The presented dynamic modeling and combination analysis are used to investigate the characteristics of the plunger valve in an actual compressor equipment. The rationality of the presented models and analysis method is verified by comparing them to measured data. Simultaneously, the varying regularity of the FSI force and flow rate is investigated while the working condition of the plunger valve is modified.

4.1 Verification of the Combination Analysis

The experiments in this paper are based on the compressor facility of the aero-engine test platform. The two-stage jet pipe servo valve in the plunger valve actuator is directly connected to the hydraulic piston cylinder. The oil pumping station can be regarded as a constant-pressure source, connected to the servo valve through a high-pressure oil supply pipe. The supply pipe is so short that the pressure drop along the pipe is negligible. The displacement transducer measures the hydraulic piston cylinder displacement and linearly converts it into a feedback current signal. To maintain the measurement accuracy, we provide a straight pipe (10D) in the downstream between the flowmeter and plunger valve.

The dynamic model established above is used to analyze the transmission mechanism. Figure 7 is a schematic diagram of the hydraulic servo system and the transmission mechanism. The specific modeling analysis parameters are shown in Table 1. In the dynamic simulation analysis, each component is assumed to be a rigid body, and constraints are applied to enable the rack and drive the piston to move in translation and the gear to rotate. A gear pair connects the rack and gear, and a rotating pair connects the crank connecting rod hinge. The rack moves at a constant speed, then the relationship between the force of the hydraulic piston, F_L, and the displacement of the hydraulic rod, x_p, is obtained.

Table 1 Modeling and analysis parameter

Module of gear		16
Number of gear teeth		30
Pitch circle diameter	/mm	450
Design stroke of hydraulic piston	/mm	340
Actual stroke of hydraulic piston	/mm	330
Actual stroke of plunger	/mm	540
Oil supply pressure	/MPa	17
Servovalve rated current	/mA	20
Servovalve rated pressure	/MPa	21
Servovalve rated flow rate	/Lmin^{-1}	210
Piston cylinder inner diameter	/mm	210
Total window area	/m^2	2.6

The properties of the window area ratio are investigated using a combination analysis in this study. It consists of a simulation of 21 sets of steady-state operating conditions for the plunger valve actuator, calculation of the corresponding window area ratio, and its comparison to the experimental steady-state data to validate the correctness of the analysis. Figure 8 shows the results of the comparative analysis. Under steady-state conditions, the maximum and average errors between experimental and simulated data are 8.432% and 2.508%, respectively. The relative error diminishes as the input window area ratio increases.

During the operation of the large compressor equipment, the window area ratio of the plunger valve must be changed frequently to adjust the flow. Therefore, the ability to effectively characterize the dynamic change in the window area ratio during the dynamic adjustment process is crucial. The change rule of the window area ratio is investigated in this section under the conditions of dynamic step and continuous change of the grid connection.

The valve outlet pressure is 15 kPa. The step control signal for the window area ratio of 21% to 36% is input at 30.5 s. The corresponding values of the window area ratio are shown in Fig. 9. According to the comparison, the experimental and simulation data are approximately 1% smaller than the input step signal in the steady state,

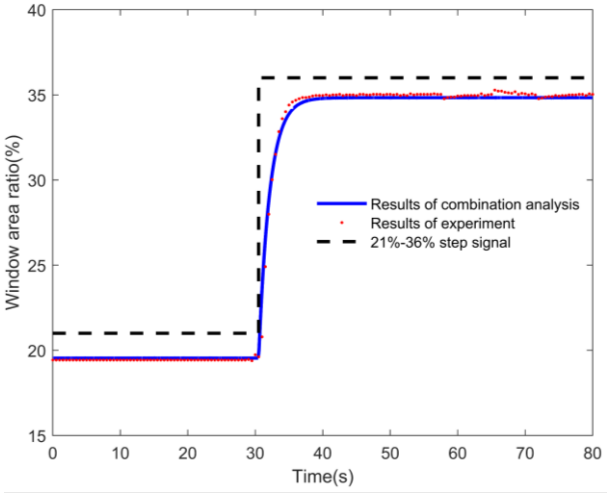

Fig. 9 Response of window area ratio under 21%-36% step signal

and the actual response is a monotonically increasing process without oscillation. The simulation value is essentially consistent with the experimental value. The adjustment time is 7 s, while the average inaccuracy is 0.85%, indicating that the servomechanism model can exactly respond to the plunger valve window area ratio under the dynamic step adjustment process.

Owing to the stringent flow rate adjustment requirements, the location of the plunger must be continually changed during the grid connection procedure to achieve an exact control of the mass flow rate and pressure in the rear cabin of the large compressor equipment. The combination analysis is used in this part to investigate the dynamic response of the valve window area ratio during the grid connection operation. Figure 10 depicts the experimental and simulated responses of the window area ratio when a continuous control signal for mesh connection is input. The trend of the simulation window area ratio is consistent with the experimental window area ratio. The simulation output can precisely follow the step and oscillation signals with an average error of 3.23% throughout the process. It shows that the

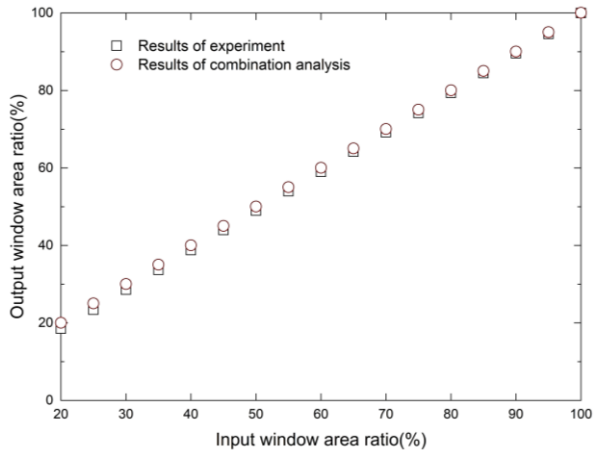

Fig. 8 Response of window area ratio in steady-state conditions

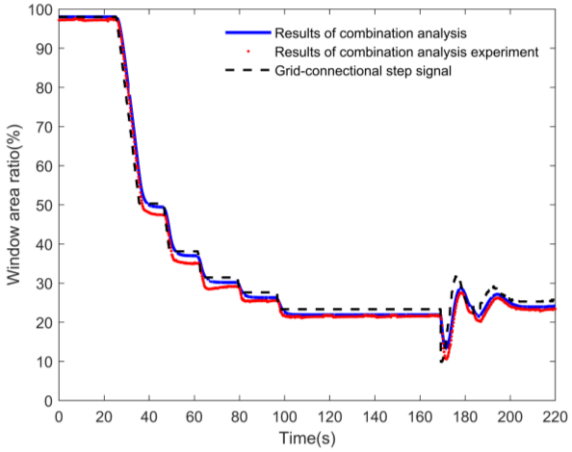

Fig. 10 Response of window area ratio of plunger valve under grid connection

Table 2 Data of mass flow rate

P_r	δ	C	Mass flow rate of the experiment	Mass flow rate of CFD	Mass flow rate of the integrated method	Relative error of the CFD simulation	Relative error of the integrated method
	(%)		(kg/s)	(kg/s)	(kg/s)	(%)	(%)
0.308	30.5	0.934	95.16	101.63	97.13	6.80	2.07
0.232	34.1	0.947	113.05	113.94	113.45	0.79	0.36
0.259	39.3	0.952	126.87	132.35	136.37	4.32	7.48
0.293	41	0.952	145.78	138.83	139.14	4.77	4.55
0.308	43.5	0.936	154.26	147.80	150.55	4.19	2.40
0.366	50.3	0.931	183.25	173.67	172.70	5.23	5.76

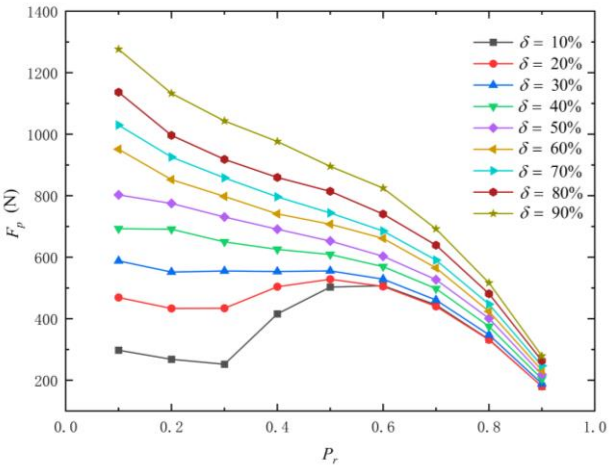

Fig. 11 FSI force characteristic under different working conditions

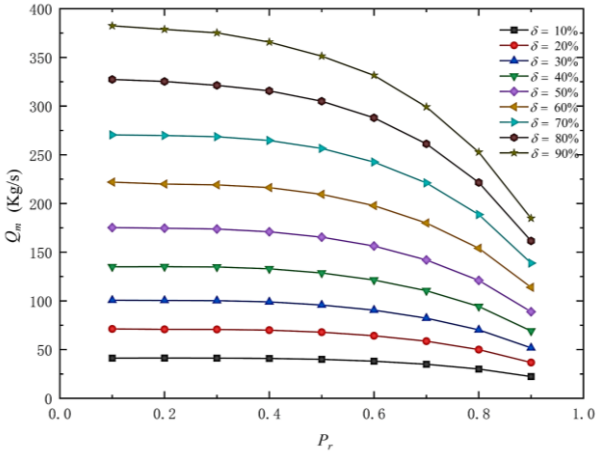

Fig. 12 Mass flow rate under different working conditions

combination method can be used to correctly analyze the dynamic properties of the valve during mesh connection.

The combination analysis and computational fluid dynamics (CFD) approach are used to calculate the mass flow rate characteristics of various window area ratios and pressure ratios. Appendix B presents details of the CFD simulation. Simultaneously, steady-state tests are carried out on the plunger valve of the real large compressor system. Table 2 compares the mass flow rates of the three approaches. The two approaches described above approach the experimental mass flow rate data well under various working situations. The average error of the combination analysis method is 3.77%, while the average error of the CFD simulation is 4.35%, which verifies the effectiveness of the combination analysis proposed in this paper and indicates that the method can meet the needs of practical engineering applications.

4.2 Influences of Parameters

According to the presented combination analysis method, the characteristics of the FSI force under various working situations are discussed in this section. The curves of the FSI force with the pressure ratio are presented in Fig. 11 for various window area ratios. The FSI force has obvious nonlinear characteristics and increases with the window area ratio. When the window area ratio is larger than 40%, the FSI force decreases as the pressure ratio increases. When the pressure ratio is smaller than 0.5, the variation trend of the differential pressure initially decreases, and then the decreasing trend of the FSI force steadily increases. When the window area ratio is smaller than 40%, the FSI force initially decreases, and then increases. The decreasing tendency is larger when the pressure ratio exceeds 0.5.

The FSI force exhibits a nonlinear changing trend when the valve operating circumstances vary, particularly at small openings. This demonstrates that the influence of the FSI force on the plunger valve cannot be ignored. This necessitates the use of the dynamic model and combination analysis described above.

As illustrated in Fig. 12, the combination analysis is used to obtain the curve of flow rate changing with the pressure ratio under varied window area ratio. There is a significant nonlinear relationship between the flow rate and pressure ratio. The flow rate increases with the window area ratio. The flow rate decreases as the pressure ratio increases at the same area ratio; the downward trend is intensified.

5. CONCLUSION

In this study, dynamic models of the plunger valve were developed, and a combination analysis method was employed as both flow and actuator were considered. To validate the efficacy of the dynamic model and

combination analysis, steady-state and transient experiments were conducted. The conclusions can be summarized as follows.

1. The comparison of the combination analysis to the experimental results showed that the dynamic models and combination analyses can precisely match the window area ratio during steady-state operations and dynamic processes such as step and compressor unit grid connection. The relative error of the mass flow rate was between 0.36% and 7.48%. The method has a good calculation accuracy and is suitable for a wide range of working conditions. The computation accuracy and convenience are superior to those of a CFD numerical simulation.
2. The combination analysis was used to analyze the relationship between the FSI force and flow rate when the pressure ratio of different window area ratios varied. At the same pressure ratio, these two parameters increased with the window area ratio. The FSI force had different variation trends on both sides of the window area ratio of 40%. Furthermore, for the same area ratio, the flow rate decreased with the increase in the pressure ratio. The decay was faster at high pressure ratios. These nonlinear properties indicate that it is necessary to perform dynamic modeling and combination analysis by considering the FSI force between the flow field and plunger.
3. The combination analysis eliminates the reliance of prior valve research on a numerical simulation and experiment, which allows to quickly and accurately output the window area ratio and mass flow rate of the plunger valve. This approach may be used as a reference for design and implementation of plunger valves in real-world applications. Furthermore, the modeling techniques described in this article may be used for various control valves.

CONFLICT OF INTEREST

The authors have no competing interests or conflicts to disclose.

AUTHORS CONTRIBUTION

Yufeng Ren: Methodology, Software, Investigation, Formal analysis, Data curation, Writing - original draft, Visualization, Writing - review & editing, Visualization. **Changqing Bai**: Conceptualization, Methodology, Writing - review & editing, Supervision. **Hongyan Zhang**: Resources, Writing - review & editing.

REFERENCE

Aboelela, M. A. S., Essa, M. E. S. M., & Hassan, M. A. M. (2018). Modeling and identification of hydraulic servo systems. *International Journal of Modelling and Simulation*, *38*(3), 139–149. https://doi.org/10.1080/02286203.2017.1405713

Ferrari, A., Pizzo, P., & Rundo, M. (2018). Modelling and experimental studies on a proportional valve using an innovative dynamic flow-rate measurement in fluid power systems. *Proceedings of the Institution of Mechanical Engineers, Part C: Journal of Mechanical Engineering Science*, *232*(13), 2404–2418. https://doi.org/10.1177/0954406217721259

Finnemore, E. J., & Franzini, J. B. (2002). *Fluid mechanics with engineering applications.* McGraw-Hill Education. https://www.accessengineeringlibrary.com/content/book/9780072432022

Gan, G., & Riffat, S. B. (1996). Measurement and computational fluid dynamics prediction of diffuser pressure-loss coefficient. 15. https://doi.org/10.1016/0306-2619(95)00078-X

Gupta, R. K., Kumar, L., & Mandal, N. P. (2019). *Displacement control of an electro- hydraulic actuator using proportional solenoid valve*. International Conference on Computing, Power and Communication Technologies (GUCON). IEEE, *2019*, 673-677. https://ieeexplore.ieee.org/abstract/document/8940360.

Jobson, D. A. (1955). On the Flow of a Compressible Fluid through Orifices. *Proceedings of the Institution of Mechanical Engineers*, *169*(1), 767–776. https://doi.org/10.1243/PIME_PROC_1955_169_077_02

Karunanidhi, S., & Singaperumal, M. (2010). Design, analysis and simulation of magnetostrictive actuator and its application to high dynamic servo valve. *Sensors and Actuators A: Physical*, *157*(2), 185–197. https://doi.org/10.1016/j.sna.2009.11.014

Kim, W., Won, D., Shin, D., & Chung, C. C. (2012). Output feedback nonlinear control for electro-hydraulic systems. *Mechatronics*, *22*(6), 766–777. https://doi.org/10.1016/j.mechatronics.2012.03.008

Morimune, T., Hirayama, N., & Maeda, T. (1980). Study of compressible high speed gas flow in piping system: 1st report, piping systems with bends or elbows. *Bulletin of JSME*, *23*(186), 1997–2004. https://doi.org/10.1299/jsme1958.23.1997

Naseradinmousavi, P., & Nataraj, C. (2011). Nonlinear mathematical modeling of butterfly valves driven by solenoid actuators. *Applied Mathematical Modelling*, *35*(5), 2324–2335. https://doi.org/10.1016/j.apm.2010.11.036

Prasad, V., Gupta, M. V., & Chaurasiya, M. P. K. (2011). Numerical derivation of flow characteristics of plunger valve. FMFP 2014. https://www.researchgate.net/publication/318653729_NUMERICAL_DERIVATION_OF_FLOW_CHARACTERISTICS_OF_PLUNGER_VALVE

Saha, B. K., Chattopadhyay, H., Mandal, P. B., & Gangopadhyay, T. (2014). Dynamic simulation of a pressure regulating and shut-off valve. *Computers & Fluids*, *101*, 233–240. https://doi.org/10.1016/j.compfluid.2014.06.011

Shao, J., Chen, L., & Sun, Z. (2005). *The application of fuzzy control strategy in electro-hydraulic servo system.* IEEE International Conference Mechatronics and Automation. https://doi.org/10.1109/ICMA.2005.1626871

Ulanicki, B., Picinali, L., & Janus, T. (2015). Measurements and analysis of cavitation in a pressure reducing valve during operation – a case study. *Procedia Engineering*, *119*, 270–279. https://doi.org/10.1016/j.proeng.2015.08.886

Valiantzas, J. D. (2008). Explicit power formula for the darcy–weisbach pipe flow equation: application in optimal pipeline design. *Journal of Irrigation and Drainage Engineering*, *134*(4), 454–461. https://doi.org/10.1061/(ASCE)0733-9437(2008)134:4(454)

Wang, G., Zhang, R., Wang, J., Wang, W., & Xie, M. (2016). *Design and analysis of plunger valve based on ansys.* Proceedings of the 2016 International Conference on Innovative Material Science and Technology (IMST 2016), Shenzhen, China. https://doi.org/10.2991/imst-16.2016.73

Wang, Y. C., Li, C., Jiang, J., Zhang, S. S., Li, Y. H., & Ying, R. (2018). Numerical simulation of plunger valve of colliding energy dissipation in the condition of low backpressure and high pressure difference. *IOP Conference Series: Earth and Environmental Science*, *163*, 012096. https://doi.org/10.1088/1755-1315/163/1/012096

Xiong, S., Wilfong, G., & Lumkes, J. (2019). Development of a novel high-speed actuation mechanism using a magneto-rheological fluid clutch and its application to a fluid control valve. *Journal of Intelligent Material Systems and Structures*, *30*(16), 2502–2516. https://doi.org/10.1177/1045389X19862368

Yao, B., Bu, F., & Chiu, G. T. C. (2001). Non-linear adaptive robust control of electro-hydraulic systems driven by double-rod actuators. *International Journal of Control*, *74*(8), 761–775. https://doi.org/10.1080/002071700110037515

Yao, B., Bu, F., Reedy, J., & Chiu, G. T.-C. (2000). Adaptive robust motion control of single-rod hydraulic actuators: Theory and experiments. *IEEE/ASME Transactions on Mechatronics*, *5*(1), 79–91. https://doi.org/10.1109/3516.828592

Yu, J., & Yu, S. (2015). Numerical and experimental research of flow and sound fields in an axial-flow check valve and its optimization. *Advances in Mechanical Engineering*, *7*(11), 1687814015619827. https://doi.org/10.1177/1687814015619827

Zheng, S., Luo, M., Xu, K., Li, X., Bie, Q., Liu, Y., Yang, H., & Liu, Z. (2019). Case study: Erosion of an axial flow regulating valve in a solid-gas pipe flow. *Wear*, *434–435*, 202952. https://doi.org/10.1016/j.wear.2019.202952

APPENDIX A

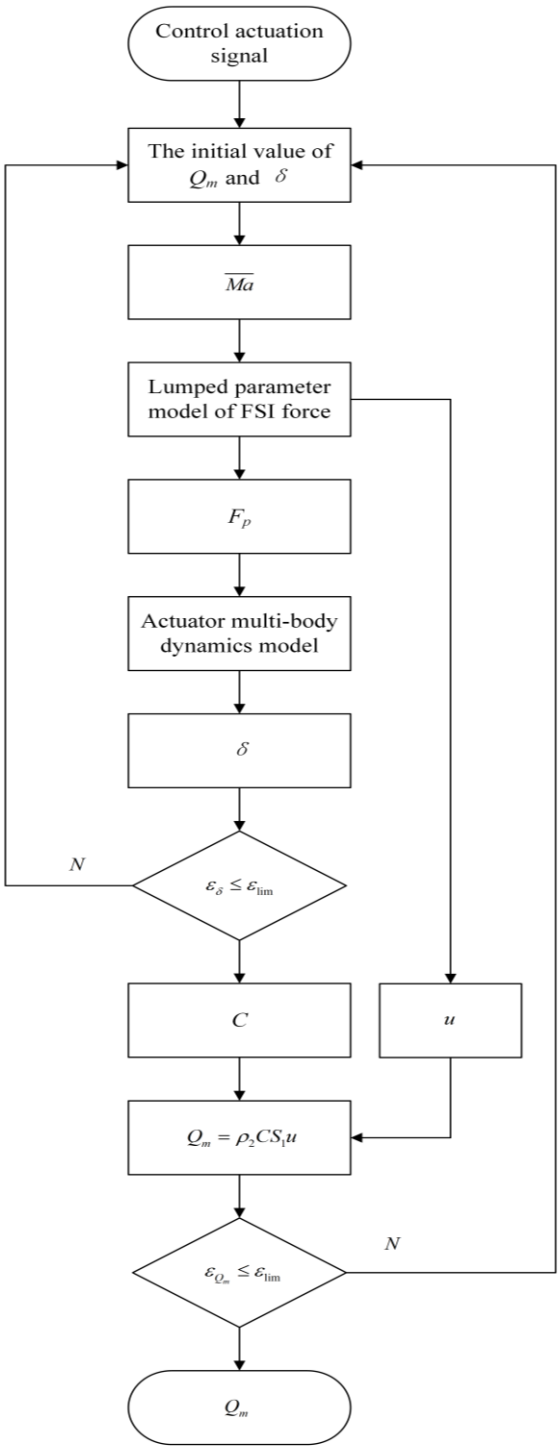

Fig. 13. Flow chart of the combination analysis.

APPENDIX B

The CFD simulation adopts the commercial CFD solver Fluent 2021 R1 based on the finite volume method. Considering the plunger valve is rotationally symmetric, a quarter model is used for fluid dynamics simulation to reduce the cost of calculation. The internal cavity of the plunger flow valve and the plunger are reasonably simplified.

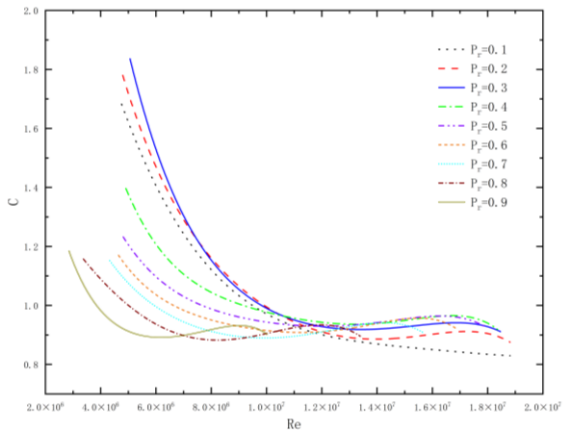

Fig. 14 Contraction coefficient varies with Reynolds number under different pressure ratios

The three-dimensional model of the plunger valve established by CATIA is shown in Fig. 15, where the plunger is simplified as a baffle moving along the axial direction. Different positions of the baffle correspond to different window areas of the plunger valve. The cup-shaped flow windows are uniformly distributed around the circumference of the guide cap so that there are 12 windows for the full valve in total. The main geometric

Fig. 15 Quarter model of the plunger valve

Table B1 Mass flow rate and error in various grid

Case	Grid number	Mass flow rate /kg·s^{-1}	ε /%
1	2974230	114.2	1.20
2	3424149	114.12	1.12
3	4262546	113.96	0.98
4	5265942	113.9	0.93

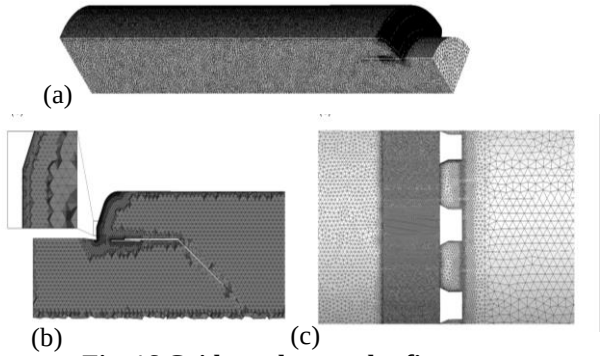

Fig. 16 Grid topology and refinement

parameters are: inlet diameter D_{in}=2.3 m, outlet diameter D_{out}=3.6 m, length of the window L=0.54 m, maximum window area is 2.61225 m^2, and the plunger stroke is 0.57 m. In order to improve the accuracy of the numerical calculation and ensure the reliability of the calculation, a pipe with a length of 1 m before the valve and a pipe with a length of 10 m after the valve are added as the calculation domain.

The calculation uses a non-structural tetrahedral grid. In order to capture the flow details of the near-wall surface of the stream, the corner wall is encrypted and the boundary layer grid is arranged. The first layer of the grid is 0.1 mm, and the boundary layer grid growth rate is 1.2, so that the y+ is always less than 30. The numbers of the grid are respectively set to 2974230, 3424149, 4262546, and 5265942 to compare and explore the influence of the grid number on the calculation accuracy. The window area ratio is set to δ=34.1 %, the pressure after the valve is atmospheric pressure, and the pressure ratio, P_r, of the pressure after the valve to the pressure before the valve is set to 0.23. Take the outlet flow as the observation value, and the comparison with the experimental observation flow rate values of 112.846 kg/s under the same working condition is shown in Table B1. The relative error between cases 3, 4 and the experimental value is less than 1 %. Case 3 is used for calculation by weighing the calculation resources and accuracy, which means the number of the grid is 4262546 for subsequent numerical calculations. When the window area ratio is 35%, the valve body and fluid domain grid of the plunger valve are shown in Fig. 16.

This study conducts a steady numerical simulation of the plunger valve. The boundary conditions at work are quite unique. The inlet connects to the atmosphere, and the exhaust pipe is connected to the compressor system. The boundary conditions of the inlet and outlet are pressure boundaries. Atmospheric pressure is the absolute pressure in front of the valve. According to the actual flow in the plunger valve, the wall boundary condition adopts the adiabatic no-slip wall, and the fluid medium adopts the ideal gas. The realizable k-ε turbulence model is used for the viscous flow calculation, and the SIMPLE algorithm is used for the pressure-velocity coupling. It is a classic and extensively used pressure-correction method in engineering CFD simulations, and it is usually used to generate the steady flow solution in CFD. The pressure item adopts the second-order scheme, and the momentum term, energy term, turbulent kinetic energy term, and turbulent dissipation term is solved by the second-order upwind scheme.

The velocity contour and the pressure contour under the condition of and are shown in Fig. 17 and Fig. 18.

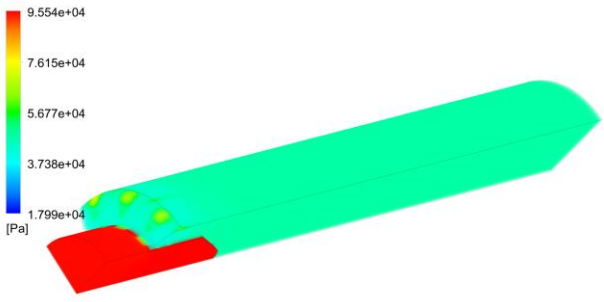

Fig. 17 Velocity contour of the plunger valve

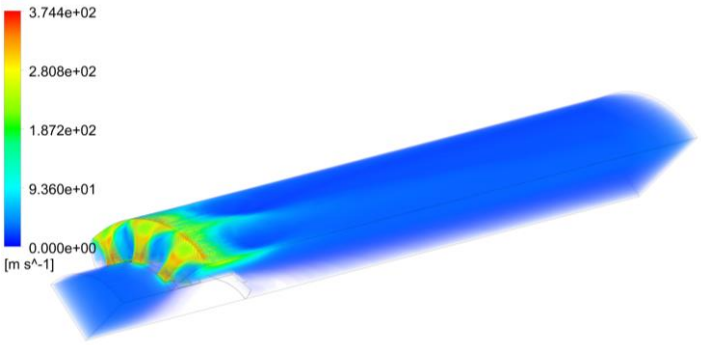

Fig. 18 Pressure contour of the plunger valve